Nuclear Science and Techniques (2024) 35:60
https://doi.org/10.1007/s41365-024-01420-6

Study on the optimal incident proton energy of ^{7}Li(p, n)^{7}Be neutron source for boron neutron capture therapy

Yi-Nan Zhu[1,2] · Zuo-Kang Lin[1,2] · Hai-Yan Yu[1] · Ye Dai[1,2] · Zhi-Min Dai[1,2] · Xiao-Han Yu[1,2]

Received: 27 August 2023 / Revised: 13 November 2023 / Accepted: 15 November 2023 / Published online: 3 May 2024

Abstract
Boron neutron capture therapy (BNCT) is recognized as a precise binary targeted radiotherapy technique that effectively eliminates tumors through the ^{10}B(n,α)^{7}Li nuclear reaction. Among various neutron sources, accelerator-based sources have emerged as particularly promising for BNCT applications. The ^{7}Li(p,n)^{7}Be reaction is highly regarded as a potential neutron source for BNCT, owing to its low threshold energy for the reaction, significant neutron yield, appropriate average neutron energy, and additional benefits. This study utilized Monte Carlo simulations to model the physical interactions within a lithium target subjected to proton bombardment, including neutron moderation by an MgF_2 moderator and subsequent BNCT dose analysis using a Snyder head phantom. The study focused on calculating the yields of epithermal neutrons for various incident proton energies, finding an optimal energy at 2.7 MeV. Furthermore, the Snyder head phantom was employed in dose simulations to validate the effectiveness of this specific incident energy when utilizing a ^{7}Li (p,n)^{7}Be neutron source for BNCT purposes.

Keywords Boron neutron capture therapy · ^{7}Li(p,n)^{7}Be neutron source · Incident proton energy · Monte Carlo simulation

1 Introduction

The concept of boron neutron capture therapy (BNCT) was first introduced by G.L. Locher in 1936 as a binary targeted radiation therapy [1]. In BNCT, compounds containing boron-10, which are non-toxic and can be normally metabolized, are administered into the human body via intravenous injection. These compounds specifically target tumor cells with minimal distribution in normal tissues. Following administration, the patient is exposed to a beam of epithermal or thermal neutrons, initiating the therapeutic process. This selective targeting approach underscores the potential of BNCT in treating various cancers with precision. The principle behind the therapeutic effects is the emission of lithium-7 and alpha particles with a high linear energy transfer (LET) as a result of the high cross section between the boron-10 nucleus and thermal neutrons. The nuclear reaction of ^{10}B(n,α)^{7}Li is described in Eq. (1). The particles released during BNCT, being smaller than a typical cell (< 10 μm), exhibit potent biological effects. Their ability to specifically target and inactivate tumor DNA while sparing normal tissue from irradiation damage is a key advantage of this therapy. As a result, BNCT has seen broad application in the treatment of various malignant tumors, such as glioblastoma multiforme (GBM), recurrent head and neck cancer, lung cancer, and liver cancer, demonstrating its effectiveness and versatility in oncology [2–6].

$$^{10}\mathrm{B} + \mathrm{n} \rightarrow ^{11}\mathrm{B} \rightarrow \alpha + ^{7}\mathrm{Li} + \gamma\,(0.48\ \mathrm{MeV})\,(93.7\%)$$

$$^{10}\mathrm{B} + \mathrm{n} \rightarrow ^{11}\mathrm{B} \rightarrow \alpha + ^{7}\mathrm{Li}\,(6.3\%) \quad (1)$$

In 1951, Sweet et al. conducted the first BNCT clinical trial based on a reactor neutron source at the Brookhaven Graphite Research Reactor (BGRR) of Brookhaven National Laboratory (BNL). After that, a series of patients with malignant brain tumors were treated with BNCT at the Brookhaven Medical Research Reactor (BMRR) from

✉ Zuo-Kang Lin
linzuokang@sinap.ac.cn

✉ Xiao-Han Yu
yuxiaohan@sinap.ac.cn

[1] Shanghai Institute of Applied Physics, Chinese Academy of Sciences, Shanghai 201800, China

[2] University of Chinese Academy of Science, Beijing 100049, China

1959 to 1961. During this same period, the Massachusetts Institute of Technology (MIT) performed clinical studies on patients using a reactor [7]. Subsequently, several countries worldwide have conducted research on reactor-based BNCT, including research conducted at the High Flux Reactor (HFR) in the Netherlands [8], FiR1 research reactor in Finland [9], LVR-15 reactor in the Czech Republic [10], Kyoto University Research Reactor (KURR) in Japan [11], RA-6 reactor in Argentina [12], and Tsing Hua Open-pool Reactor (THOR) in Taiwan, China [13]. This research has yielded a series of valuable BNCT clinical results, and BNCT has reached a new stage during this period. However, because of the shortcomings of using a reactor located far from the hospital, along with the high costs of maintenance, low acceptance by the public, and other unfavorable factors, the development of reactor-based BNCT stagnated in the late twentieth century. Accelerator-based BNCT (AB-BNCT) neutron sources have gradually replaced reactor neutron sources, and this type of therapy has rapidly developed in recent years. In Japan, the first commercial AB-BNCT facility was designed and constructed by Kyoto University and Sumitomo Heavy Industries, Ltd. A system was built at the Southern Tohoku BNCT Research Center using a cyclotron-based epithermal neutron source (C-BENS) producing a proton beam with an energy of 30 MeV and a current of 2 mA, which is used to bombard a beryllium target. On March 2020, a BNCT system (NeuCure™ System) and dose calculation program (NeuCure™ Dose Engine) were approved by the Japanese Ministry of Health, Labor and Welfare [14, 15]. In addition, the University of Tsukuba and National Cancer Center are also conducting an AB-BNCT project, which is called iBNCT. The energy of the incident proton beam is 8 MeV, and its current intensity is 5 mA. The target material is beryllium, and this facility has been in operation since 2016 [16]. AB-BNCT research is also being performed at the University of Helsinki in Finland. A 2.6 MeV, 30 mA compact linear accelerator-based neutron source with a rotating lithium target was installed in 2018. Clinical trials with patients with recurrent head and neck cancer are about to begin if approved by the Finnish health authorities [17]. In China, the Spallation Neutron Source (SNS) team has been working on an AB-BNCT project called D-BNCT, which involves a proton energy of 2.8 MeV and current of 20 mA. D-BNCT will be applied to BNCT research as soon as possible [18, 19]. The Xiamen Humanity Hospital (XHH) BNCT Center has developed a tandem accelerator with vacuum insulation and a solid lithium target bombarded by a 2.5 MeV, 10 mA proton beam. All of these AB-BNCT facilities have been tested, and the medical BNCT system NeuPex, which was developed by NEUBRON, began registration testing in March 2023 in preparation for the acceptance of patients [20].

In AB-BNCT, neutrons are obtained by accelerating charged particles and bombarding a target. Based on the different reaction channels between the accelerated charged particles and target, the main types of accelerator-based neutron sources include (p,n), (d,n), (d,d), (d,t), and other patterns [21–23]. Related research indicates that a proton-driven accelerator neutron source based on the (p, n) reaction has the advantages of a high neutron yield, suitable average neutron energy, and easy moderation of the fast neutrons generated by the target bombardment to the epithermal neutron energy region (0.5–10 keV) applicable to BNCT [24]. Therefore, it is the most promising accelerator-based neutron source in BNCT commercial application. The selection of the target material is a key issue. Blistering and cooling are two crucial factors to be considered in the design of the target. Lithium and beryllium are the two main neutron production target materials commonly used for neutron sources based on the (p, n) reaction [25, 26]. It is well known that the neutron yield of a lithium target in a low incident proton energy range of less than 10 MeV is higher than that of beryllium [27]. Increasing the incident proton energy increases the cost of the accelerator. Thus, in the low incident proton energy range, the performance of a lithium target is superior to that of a beryllium target.

The current study primarily focuses on investigating a proton-driven accelerator-based neutron source utilizing a lithium target. The study emphasizes how variations in the energy of incident proton beams give rise to distinct physical characteristics in the resulting neutrons produced by bombardment. Furthermore, these energy variations have a significant impact on subsequent neutron moderation, ultimately shaping the spectrum of the therapeutic neutron beam and influencing therapeutic outcomes. The main objective of this study is to propose a proton accelerator-driven neutron source with an optimal incident proton energy tailored for BNCT applications. This study aims to serve as a valuable reference for the future development of commercial AB-BNCT facilities. Throughout the calculations, the Monte Carlo program MCNPX [28], coupled with the JEFF3.1 database, was employed. To ensure statistical accuracy within a 3% error margin, variance reduction techniques such as geometry splitting and roulette were utilized, with a total of 5×10^8 histories considered.

2 Materials and methods

2.1 Incident protons and lithium target parameters

In this study, the physical dynamics of target bombardment were simulated using a unidirectional parallel proton beam. A threshold energy of 1.88 MeV for the ^{7}Li(p,n)^{7}Be reaction was referenced from the Evaluated Nuclear Data File

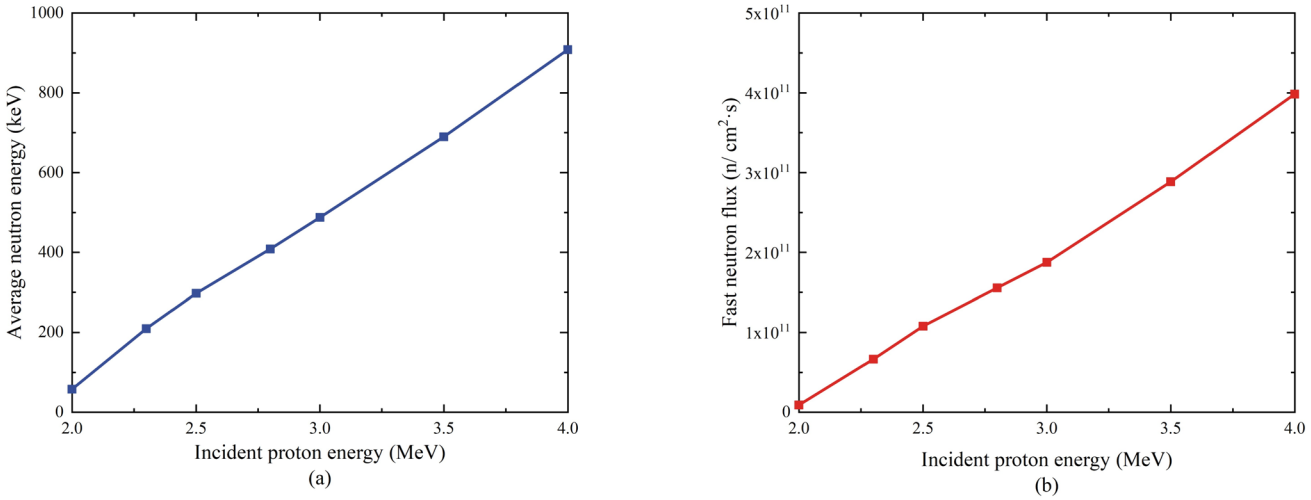

Fig. 1 **a** Average neutron energy after bombardment of lithium target by protons with different energies; **b** Fast neutron flux values at different incident proton energies with 10 mA beam intensity

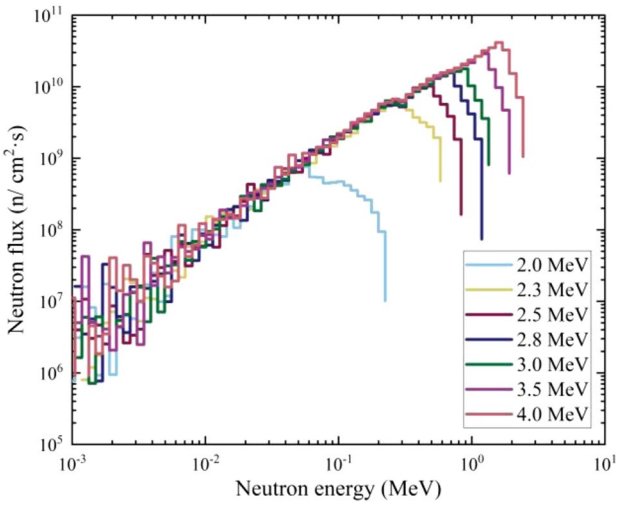

Fig. 2 (Color online) Neutron spectra under different incident proton energies

(ENDF) [29]. Figure 1a illustrates the average neutron energies resulting from various incident proton energies within the 2.0–4.0 MeV range. A clear trend was observed where the average neutron energy rose consistently with increasing proton energy, yet remained below 1.0 MeV for proton energies up to 4.0 MeV, the average energy of the produced neutrons did not exceed 1.0 MeV. Figure 1b shows the fast neutron flux after incident protons with different energies bombarded lithium targets with a 10 mA beam intensity. Additionally, Fig. 2 depicts the neutron spectra for incident proton energies ranging from 2.0 to 4.0 MeV, showing that both the spectrum and total neutron flux increase with proton energy. However, excessively high neutron energies complicate their moderation to the epithermal range suitable for BNCT. Consequently, to maintain neutron energies within a manageable range for BNCT, this study restricted incident proton energies to 2.0–4.0 MeV and set the beam intensity at 10 mA.

Notably, with an appropriate lithium target thickness, neutron yield increased as the incident proton energy rose from 2.0 to 4.0 MeV. To optimize neutron production, simulations were conducted on bombarding a lithium target with protons at an incident energy of 4.0 MeV and a beam radius of 3 cm. The energy deposition in the lithium target by a 4.0 MeV proton beam is depicted in Fig. 3, where a notable Bragg Peak is observed at the end of the proton's trajectory. To prevent target blistering and enhance heat dissipation, the Bragg Peak's position was strategically placed outside the target's main body. The simulation showed that the Bragg Peak occurred at a lithium target thickness of approximately 450 μm for a 4.0 MeV proton beam. Consequently, to meet the objectives and ensure adequate neutron yields for protons up to 4.0 MeV, the lithium target was designed with a thickness of 500 μm and a radius of 8 cm for further calculations.

2.2 BSA model for Monte Carlo simulation

A beam shaping assembly (BSA) is designed to transform the fast neutrons produced by proton bombardment into an epithermal neutron beam suitable for BNCT applications. Figure 4 presents a sectional view of a BSA, with the proton beam directed positively along the X-axis. The BSA consists of a cylindrical structure that includes a moderator, reflector, thermal neutron absorption layer, gamma-ray shielding layer, and collimator. The reflector surrounds the moderator and the proton beam channel, reflecting neutrons back into the moderator

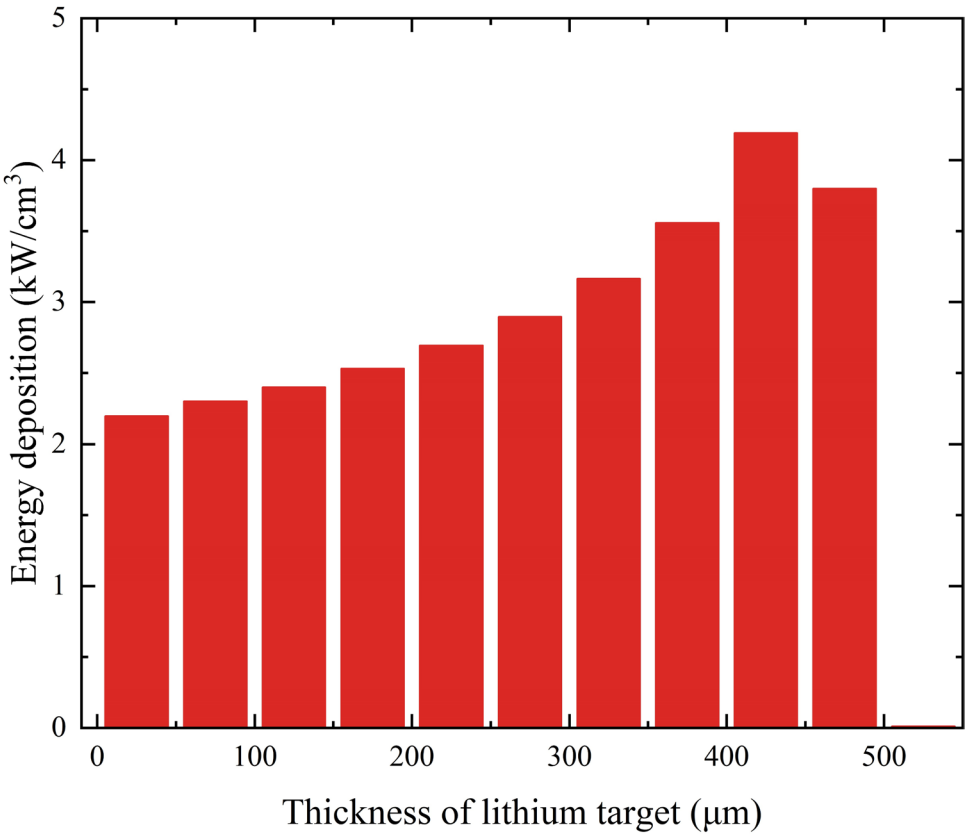

Fig. 3 Energy deposition in the lithium target with an incident proton energy of 4.0 MeV

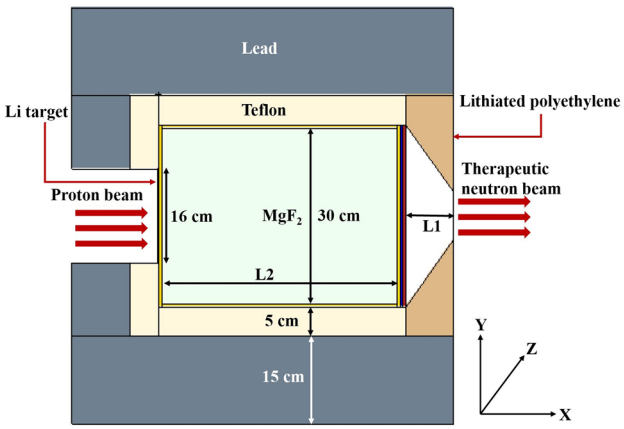

Fig. 4 (Color online) Sectional view of BSA

to enhance the epithermal neutron flux at the BSA outlet. Suitable reflector materials are those with high elastic scattering and low absorption cross sections in the epithermal neutron energy range. During neutron moderation, thermal neutrons will be obtained and gamma-rays will be released. Hence, the thermal neutron absorption layer and gamma shielding layer are designed to protect healthy tissues from damage. A collimator shapes and directs the therapeutic neutron beam, minimizing neutron scattering outside the treatment area by absorbing the off-target emissions. The BSA's design features include an 8 cm radius lithium target with a 500 μm thickness, surrounded by a 0.5 cm aluminum-wrapped moderator with a 15 cm radius located behind the target. Following the moderator, 0.5 cm lithium fluoride (LiF) thermal neutron absorption layer and a 0.5 cm bismuth gamma-ray shielding layer are sequentially positioned. LiF was chosen for its high thermal neutron absorption capability, and bismuth for its effective gamma-ray shielding. Surrounding the moderator radially were two types of reflectors made from lead and Teflon, chosen for their favorable scattering and absorption properties in the epithermal neutron energy range, with radii set at 15 cm and 5 cm, respectively. The collimator, composed of lithiated polyethylene with a 7% lithium-6 content, utilized Hydrogen-1's low atomic mass to efficiently slow down neutrons for absorption by lithium-6. The therapeutic neutron beam's exit to the bismuth gamma-ray shielding layer was set at a distance of 8 cm (L1), with the beam outlet also measuring 8 cm in diameter. The moderator is the core component of the entire BSA design. Its primary role is to reduce the energy of fast neutrons into the epithermal neutron energy range through the scattering effect. Many contributions to the design of moderators based on ^{7}Li (p, n)^{7}Be reactions have been made [30–32]. Generally, a good moderator needs a higher scattering cross section in the fast neutron energy region and a lower absorption cross section in the epithermal neutron energy region

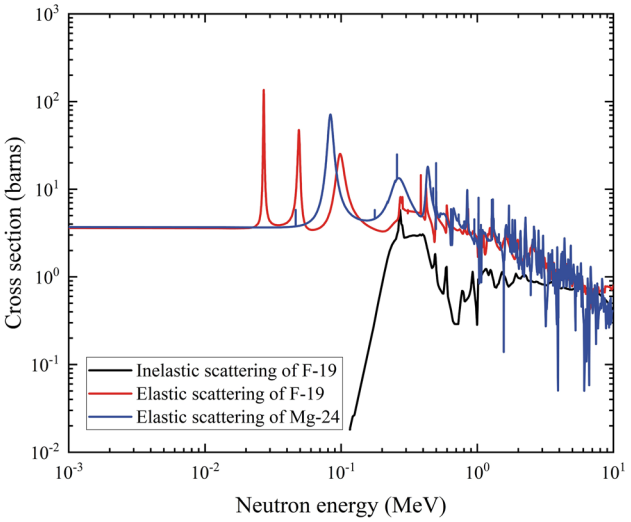

Fig. 5 (Color online) Scattering cross sections of fluorine-19 and magnesium-24

Table 1 Densities of materials used in BSA facility components

Material	Density (g/cm^3)
Al	2.70
Bi	9.80
LiF	2.64
Lithiated polyethylene	0.98
MgF_2	3.15
Pb	11.35
Teflon	2.25

[33]. For neutrons generated from the ^{7}Li(p,n)^{7}Be reaction, fluorine-19 and magnesium-24 have complementary scattering resonance peaks in the desired energy region, which is beneficial for moderating. The scattering cross sections of fluorine-19 and magnesium-24 are shown in Fig. 5. Moreover, MgF_2 has a low cost, stable properties, and no long-life radionuclides after irradiation. Thus, MgF_2 was employed as the moderator in this research, and its thickness (L2) was optimized for a series of incident proton energies from 2.0 to 4.0 MeV in the subsequent simulations. Table 1 lists the materials used for all of the BSA facility components, along with their densities.

3 Results and discussion

3.1 Search for optimum incident proton energy

In general, the neutron flux is an important parameter of a neutron radiation field, especially the flux of epithermal neutrons, which plays a primary role in the BNCT procedure [34]. Therefore, the proportion and absolute flux of epithermal neutrons determine the quality of the therapeutic neutron beam. The International Atomic Energy Agency (IAEA) has provided recommended values for therapeutic neutron beams in TECDOC-1223, including values for the absolute flux of epithermal neutrons (Φ_{epi}), the fast neutron component of a therapeutic neutron beam (D_{fast}/Φ_{epi}), gamma-ray component of a therapeutic neutron beam (D_{γ}/Φ_{epi}), ratio of the epithermal neutron flux to thermal neutron flux (Φ_{epi}/Φ_{th}), and ratio of the neutron current to total neutron flux (J/Φ) [35]. Although the ratio of the epithermal neutron flux to total neutron flux is not clearly listed in these recommended values, this parameter (Φ_{epi}/Φ_{total}) is non-ignorable and significant. It is worth mentioning that this parameter has also been used as a standard for evaluating the quality of therapeutic neutron beams in recent research [36]. Therefore, this standard was also adopted as a main indicator of whether the therapeutic neutron beam reached the optimal moderating state under the conditions of different incident proton energies in this work.

Figure 6a shows the ratio of the epithermal neutron flux to total neutron flux with an MgF_2 moderator for seven typical incident proton energy values. The trend for the change in the ratio of the epithermal neutron flux to total neutron flux with the thickness of the moderator was first to increase to a peak and then decrease for all of the incident proton energy values. Obviously, excessive moderation would reduce the quality of the therapeutic neutron beam as a result of unexpected neutron scattering and absorption effects. As the energy of the incident proton increased, the thickness of the moderator needed to reach the optimal moderating state also continuously increased. This was consistent with the previously described conclusion that the difficulty of moderation increases with the incident proton energy. In Fig. 6a, the peaks for the ratio of epithermal neutrons to total neutrons have been marked with colored arrows, and the details are listed in Table 2. Moreover, other neutron beam quality parameters for these incident proton energy values at their optimal moderating states and the recommended values from IAEA are also presented in Table 3. As can be seen from Table 3, all seven incident proton energies could basically meet the values recommended by IAEA for the therapeutic neutron beam parameters from the BSA exit at their optimal moderating states, except for the ratio of epithermal neutrons to thermal neutrons when the incident proton energy was greater than 3.0 MeV, and the situation where the absolute flux of epithermal neutrons was insufficient when the incident proton energy was less than 2.3 MeV.

As an evaluation criterion, it was determined that the neutron beam had reached the optimal moderating state when the proportion of epithermal neutrons reached its highest value. We used these data points at the optimal moderating states and the curve fit by the optimal thicknesses of the

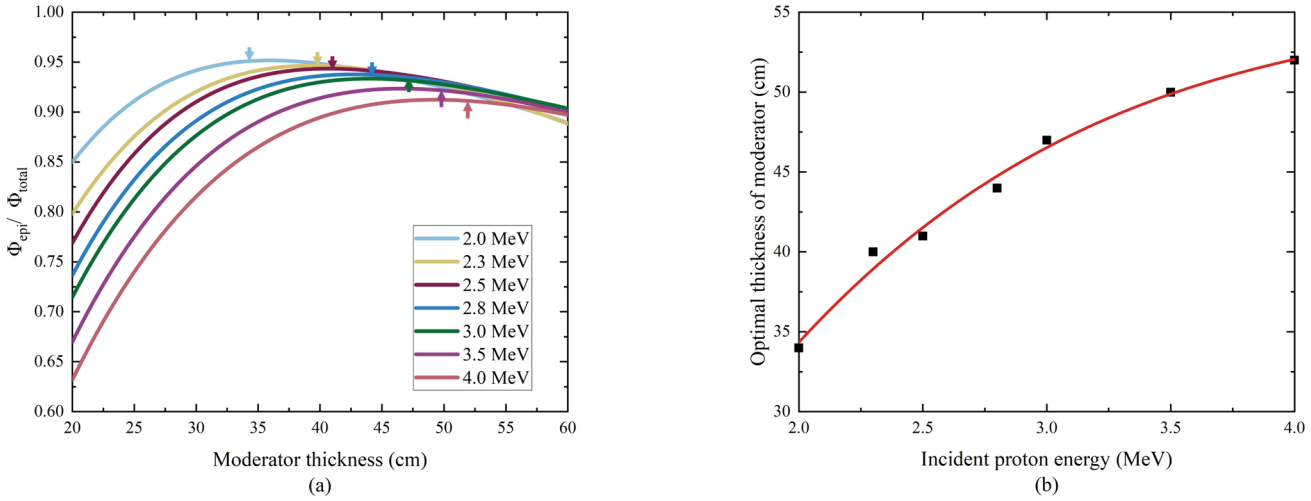

Fig. 6 (Color online) **a** Variation of ratio of epithermal neutron flux to total neutron flux with the thickness of the moderator for seven typical incident proton energies; **b** Optimal moderator thicknesses for incident proton energies from 2.0 to 4.0 MeV

Table 2 Optimal MgF_2 thickness and neutrons ratios for different incident proton energies

Parameter	Incident proton energy (MeV)						
	2.0	2.3	2.5	2.8	3.0	3.5	4.0
Optimal thickness L2 (cm)	34	40	41	44	47	50	52
Φ_{epi}/Φ_{total}	0.953	0.948	0.942	0.939	0.934	0.923	0.912
Relative error (%)	2.88	1.66	1.31	1.16	1.18	1.09	0.96

Table 3 Neutron beam quality metrics for various incident proton energies at their optimal moderating states and IAEA recommended values

Incident proton energy (MeV)	Φ_{epi} ($cm^{-2}\ s^{-1}$)	D_{fast}/Φ_{epi} ($Gy{\cdot}cm^2$)	D_γ/Φ_{epi} ($Gy{\cdot}cm^2$)	Φ_{epi}/Φ_{th}	J/Φ
2.0	1.34×10^8	1.92×10^{-15}	7.18×10^{-14}	39.4	0.707
2.3	3.98×10^8	2.03×10^{-15}	1.08×10^{-13}	28.1	0.707
2.5	6.06×10^8	2.23×10^{-15}	1.11×10^{-13}	26.4	0.706
2.8	6.83×10^8	2.69×10^{-15}	1.22×10^{-13}	22.8	0.706
3.0	6.74×10^8	3.26×10^{-15}	1.40×10^{-13}	19.8	0.706
3.5	7.86×10^8	5.76×10^{-15}	1.59×10^{-13}	17.9	0.706
4.0	9.08×10^8	1.08×10^{-14}	1.78×10^{-13}	17.0	0.703
IAEA recommend value	$>5\times10^8$	$<2\times10^{-13}$	$<2\times10^{-13}$	>20	>0.7

moderator for incident proton energies from 2.0 to 4.0 MeV, as presented in Fig. 6b. At this point, we could obtain all of the moderator thicknesses where the optimal moderating state was reached with incident proton energies from 2.0 to 4.0 MeV. Under the condition of the optimal moderating state, the ratios of the epithermal neutron flux to total neutron flux of protons with incident energy values ranging from 2.0 to 4.0 MeV in 0.1 MeV steps are presented in Fig. 7. On the whole, the proportion of epithermal neutrons at the optimal moderating state tended to decrease with an increase in the incident proton energy. However, the difference between the maximum and minimum values for the ratio of the epithermal neutron flux to total neutron flux did not exceed 5%, which showed that there were only slight differences. It is important to highlight that the ratio of epithermal neutron flux to total neutron flux is critical for assessing the effectiveness of therapeutic neutron beams for therapeutic use, particularly as this ratio approaches critical values. To identify the most effective proton energy for neutron production, we also examined the absolute flux of epithermal neutrons at the BSA outlet across the same range of incident proton energies, under optimal conditions. In the

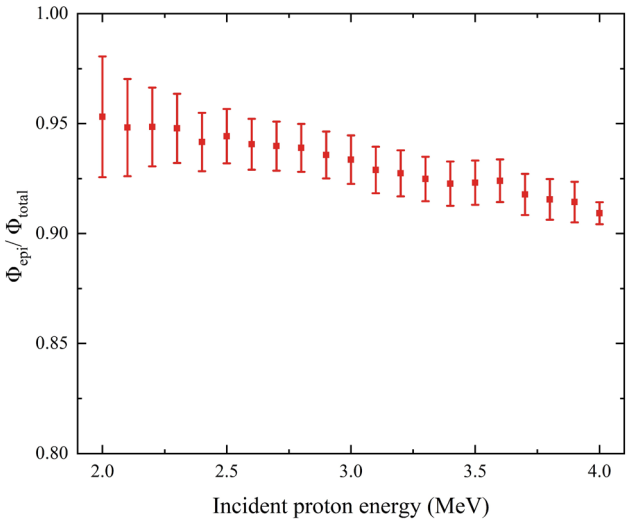

Fig. 7 Ratios of epithermal neutron flux to total neutron flux at optimal moderating states

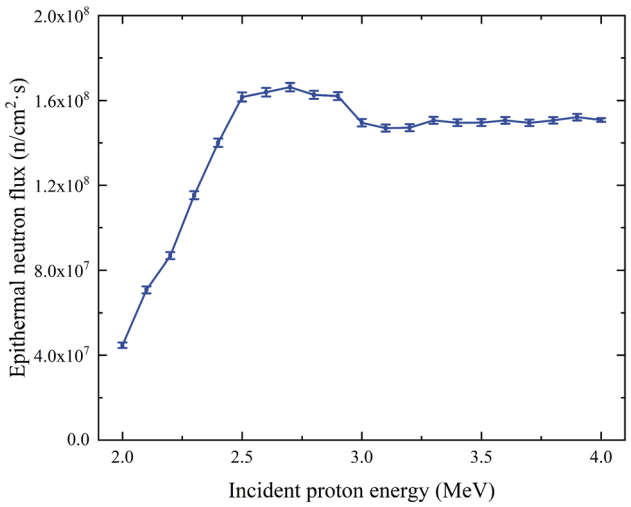

Fig. 8 Absolute flux of epithermal neutrons generated by protons per unit of energy at the optimal moderating state

context of BNCT, managing the heat produced in neutron generation targets is crucial. The use of lithium in the (p, n) reaction poses challenges due to its low melting point, which is a limitation for accelerator-based neutron sources. Thus, the efficiency of epithermal neutron production per unit of proton energy is a more suitable metric for evaluating the quality of the therapeutic neutron beam, as shown in Fig. 8.

As depicted in Fig. 8, there exists a favorable range for the absolute epithermal neutron flux per unit of energy when the incident proton energy falls between 2.5 and 2.9 MeV. Beyond an incident proton energy of 2.9 MeV, there is a noticeable decline in the absolute epithermal neutron yield per unit of energy. The most appealing finding is the peak value, which reaches 1.66×10^{8}/cm^{2}·s at an incident proton energy of 2.7 MeV. For the sake of comparison, the absolute epithermal neutron flux per unit of energy at 2.7 MeV incident proton energy is 3.7 times greater than that at 2.0 MeV. Furthermore, the difference in the ratios of epithermal neutron flux to total neutron flux between 2.0 and 2.7 MeV incident proton energies is less than 1.4%. Consequently, an incident proton energy of 2.7 MeV is deemed the most advantageous choice.

3.2 Verification of optimal incident proton energy using Snyder head phantom

To verify the therapeutic effect of the optimal incident proton energy of 2.7 MeV, a universal standard Snyder head phantom was used for dose analysis. The elemental composition of the Snyder head phantom was based on the ICRU 46 report, with the values listed in Table 4 [37]. In addition, the geometric dimensions of the Snyder head phantom are described in Eq. (2) [38].

$$\text{Brain}: \left(\frac{x}{6}\right)^2+\left(\frac{y}{9}\right)^2+\left(\frac{z-1}{6.5}\right)^2=1$$

$$\text{Skull}: \left(\frac{x}{6.8}\right)^2+\left(\frac{y}{9.8}\right)^2+\left(\frac{z}{8.3}\right)^2=1$$

$$\text{Skin}: \left(\frac{x}{7.3}\right)^2+\left(\frac{y}{10.3}\right)^2+\left(\frac{z}{8.8}\right)^2=1 \quad (2)$$

Several figures of merit (FOMs) were computed to serve as benchmarks for assessing the quality of the therapeutic neutron beam. The key FOMs are described as follows. The advantage depth (AD) is defined as the depth at which the dose within a tumor equals the maximum dose in normal tissues. This parameter reflects the penetration capability of the therapeutic neutron beam. The treatable depth (TD) represents the depth at which the tumor dose equals twice the maximum dose in normal tissues. The therapeutic ratio (TR) is a valuable metric used to characterize the ratio of the peak dose in a tumor to the peak dose in normal tissues. This metric effectively reflects the specific efficacy of therapeutic neutron beams in eradicating tumors under identical irradiation conditions. The advantage depth dose rate (ADDR) denotes the maximum dose rate delivered to normal tissues. The treatment time (TT) could be estimated as the time to reach the maximum allowable equivalent dose (D_{Eq}) of 12.5 Gy in normal tissues [39].

During the BNCT procedure, there were four types of dose contributions. The boron dose (D_B) was the component that dominated the dose contribution and was generated by high LET particles released through the ^{10}B(n,α)^{7}Li reaction between the neutrons and boron-10 compound. The thermal

Table 4 Proportion of each element (mass%) in adult head from ICRU 46

	H	C	N	O	Na	Mg	P	S	Cl	K	Ca
Brain	10.7	14.5	2.2	71.2	0.2	–	0.4	0.2	0.3	0.3	–
Skull	5.0	21.2	4.0	43.5	0.1	0.2	8.1	0.3	–	–	17.6
Skin	10.0	20.4	4.2	64.5	0.2	–	0.1	0.2	0.3	0.1	–

neutron dose (D_{th}) was attributed to the $^{14}N(n,p)^{14}C$ reaction between the thermal neutrons and nitrogen-14 nuclei, which released 0.66 MeV of energy. The fast neutron dose (D_{fast}) was produced by the elastic scattering of fast neutrons and recoil protons through the $^{1}H(n,n)p$ reaction. There were two channels for gamma-ray dose (D_{γ}) generation. One was the result of the gamma-rays existing in the therapeutic neutron beam at the outlet of the BSA. The other was from the hydrogen capture effect between the neutrons and hydrogen-1 nuclei through the $^{1}H(n,\gamma)^{2}H$ reaction [40].

The calculation of the dose distribution in the Snyder phantom was divided into the following two steps. First, the therapeutic neutron beam at the exit of the BSA was defined as the source pattern of the phantom irradiation. The F4 tally card and DE/DF card with the kinetic energy released in material (KERMA) factor were used to calculate the absorbed dose in each cell of the phantom. Then, the absorbed dose of each component was weighted and summed using Eq. (3) to obtain the equivalent biological dose [41].

$$D_{Eq} = \text{CBE factor} \times D_B + \omega_{th} \times D_{th} + \omega_{fast} \times D_{fast} + \omega_{\gamma} \times D_{\gamma} \quad (3)$$

The compound biological effectiveness (CBE) factor is characterized by values of 1.3 in normal tissues and 3.8 in tumors. Furthermore, the relative biological effect (RBE) factors, ω_{th}, ω_{fast}, and ω_{γ}, serve as weighting factors for thermal neutrons, fast neutrons, and gamma-rays, respectively. These factors were assigned values of 3.2, 3.2, and 1.0, respectively, in the dose calculation [42]. It was assumed that boron-10 compound concentrations were 10 ppm in normal tissues and 35 ppm in tumors.

Figures 7 and 8 illustrate that the highest epithermal neutron to total neutron ratio in the optimal moderating state was achieved with an incident proton energy of 2.0 MeV. However, the absolute epithermal neutron flux remained suboptimal. To determine whether the ratio of epithermal neutrons to total neutrons or the absolute flux of epithermal neutrons was the key parameter determining the therapeutic efficiency of BNCT, an incident proton energy of 2.0 MeV was employed as one of the validation cases. In addition, incident proton energies of 2.3 MeV and 3.0 MeV after interpolation were also considered. These verification cases with incident proton energies of 2.0 MeV, 2.3 MeV, and 3.0 MeV were compared with the case using 2.7 MeV. Figure 9a presents the spectra of therapeutic neutron beams at the outlet of the BSA for incident proton energies of 2.0 MeV, 2.3 MeV, and 2.7 MeV after optimal moderation. Furthermore, Fig. 9b displays the dose distributions of these therapeutic neutron beams in the Snyder head phantom, with corresponding FOMs provided in Table 5.

It is evident that the values of AD, TD, and TR with incident proton energies of 2.0 MeV, 2.3 MeV, 2.7 MeV, and 3.0 MeV exhibit remarkable proximity due to the similarity of their spectra in the epithermal neutron energy region. Nevertheless, with an incident proton energy of 2.7 MeV, TT was 40.9 min, which amounts to an 81% reduction compared to the TT with an incident proton energy of 2.0 MeV. In the context of BNCT procedures, it is imperative for the TT to be within an acceptable range. Therefore, based on this observation, it can be concluded that the absolute epithermal neutron flux plays a pivotal role in enhancing the therapeutic effectiveness of BNCT treatment, provided that the proportion of epithermal neutrons in the total neutron population does not exhibit a significant difference. The TT with an incident proton energy of 2.3 MeV was 73.7 min, which was between the values with 2.0 MeV and 2.7 MeV. As for the incident proton energy of 3.0 MeV, TT only decreased by 3.5% compared to that with 2.7 MeV. However, a higher incident proton energy made the heat dissipation of the target and neutron moderating process more difficult Furthermore, it is noteworthy that the absolute epithermal neutron flux per unit of energy for incident protons at 3.0 MeV was lower than that for 2.7 MeV. As a result, the incident proton energy of 2.7 MeV was deemed to be the optimal choice for AB-BNCT, primarily relying on the $^{7}Li(p,n)^{7}Be$ reaction.

Figure 10a and b illustrates the distribution and relative proportions of four distinct types of dose contributions within tumors, as observed in the Snyder head phantom at an incident proton energy of 2.7 MeV. Notably, the boron dose emerged as the predominant component among the dose types. This boron dose peaked at a depth of 2.4 cm within the phantom, showcasing an initial increase up to this point followed by a gradual decline as the depth further increased beyond this point. In the shallower regions, closer to the skin, the fast neutron dose was more pronounced, but its significance and proportion dwindled with increasing depth. The thermal neutron dose maintained a steady contribution of approximately 2% across all depths within the phantom. In contrast, the gamma-ray dose, which was the second-largest contributor after the boron dose, showed a marked

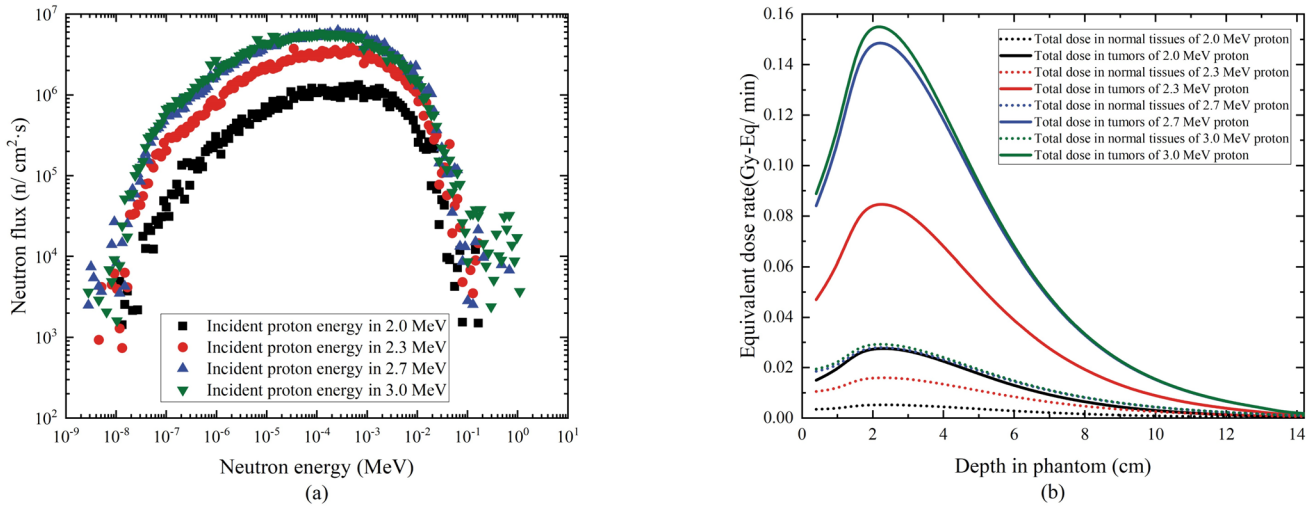

Fig. 9 (Color online) **a** Spectra of therapeutic neutron beams with incident proton energies of 2.0 MeV, 2.3 MeV, 2.7 MeV, and 3.0 MeV at their optimal moderating states; **b** Dose distributions in the Snyder head phantom

Table 5 Performance metrics for therapeutic neutron beams at optimal moderating states with varied incident proton energies

Incident proton energy (MeV)	AD (cm)	TD (cm)	TR	ADDR (Gy-Eq/min)	TT (min)
2.0	8.5	6.6	5.30	0.06	223.0
2.3	8.5	6.6	5.32	0.17	73.7
2.7	8.4	6.5	5.33	0.29	42.4
3.0	8.3	6.4	5.31	0.31	40.9

increase in its proportion for tumor depths exceeding 4 cm, highlighting its growing significance with depth.

4 Conclusion

In this study, we utilized a lithium target with an 8 cm radius and a 500 μm thickness to generate neutrons. To avoid excessively high average neutron energies and to economize on moderation, we limited the range of incident proton energies to 2.0–4.0 MeV. MgF_2 was selected as the moderator due to its superior moderation capabilities and other beneficial

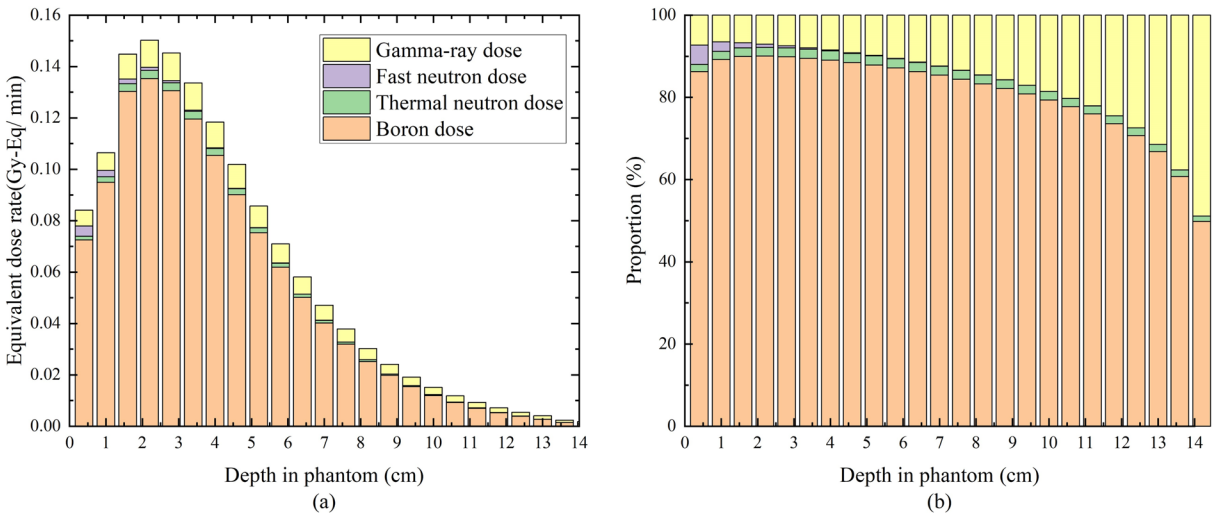

Fig. 10 (Color online) **a** Four types of dose contributions in tumors using Snyder head phantom at an incident proton energy of 2.7 MeV; **b** Dose proportions at each depth of tumor in the Snyder head phantom at an incident proton energy of 2.7 MeV

properties. The optimal moderation conditions for a BSA with varying proton incident energies were identified by maximizing the ratio of epithermal neutron flux to the total neutron flux. Furthermore, we compared the parameters of therapeutic neutron beams at the BSA exit for seven proton energy levels, ranging from 2.0 to 4.0 MeV, against the IAEA recommended values, finding the results to be broadly satisfactory. Optimal moderation thicknesses for proton energies between 2.0 and 4.0 MeV were established through curve fitting and analysis. At the optimal moderation condition, the epithermal neutron flux per unit energy peaked at an incident proton energy of 2.7 MeV, with notable benefits observed for energies between 2.5 and 2.9 MeV. A Snyder head phantom was employed to assess the therapeutic efficacy of varying proton incident energies, including a validation case at 2.0 MeV and interpolated energies at 2.3 MeV and 3.0 MeV for comparison with 2.7 MeV. The analysis revealed a significant advantage in TT at 2.7 MeV, while other FOMs showed no substantial differences. The study also detailed the four types of dose contributions and their proportions within tumors in the Snyder head phantom. Finally, it could be concluded that a proton energy of 2.7 MeV is the optimal incident energy for AB-BNCT based on the ^{7}Li(p,n)^{7}Be neutron source. In the future, an incident proton energy of 2.7 MeV may become the mainstream for the construction of a commercial AB-BNCT facility based on a ^{7}Li(p,n)^{7}Be neutron source.

Author contributions All authors contributed to the study conception and design. Material preparation, data collection and analysis were performed by YNZ, ZKL and HYY. Software was provided by YD. The first draft of the manuscript was written by YNZ and all authors commented on previous versions of the manuscript. All authors read and approved the final manuscript.

Data availability The data that support the findings of this study are openly available in Science Data Bank at and https://doi.org/10.57760/sciencedb.j00186.00419.

Declarations

Conflict of interest The authors declare that they have no competing interests.

References

1. G.L. Locher, Biological effects and therapeutic possibilities of neutrons. Am. J. Roentgenol. Radium Ther. **36**, 1–13 (1936)
2. S. Wang, Z.C. Zhang, L.L. Miao et al., Boron neutron capture therapy: Current status and challenges. Front. Oncol. **12**, 788770 (2022). https://doi.org/10.3389/fonc.2022.788770
3. M.A. Dymova, S.Y. Taskaev, V.A. Richter et al., Boron neutron capture therapy: Current status and future perspectives. Cancer Commun. **40**, 406–421 (2020). https://doi.org/10.1002/cac2.12089
4. K. Nedunchezhian, N. Aswath, M. Thiruppathy et al., Boron neutron capture therapy—a literature review. J. Clin. Diagn. Res. (2016). https://doi.org/10.7860/JCDR/2016/19890.9024
5. Z.K. Liu, W.S. Cheng, W.S. Wu et al., Principles and clinical application of boron neutron capture therapy. Med. J. Peking Union Med. Coll. Hosp. **14**, 698–705 (2023). https://doi.org/10.12290/xhyxzz.2023-0120
6. S.H. Zhu, X.L. Sun, Y.J. Zeng et al., Problems and prospects of clinical trials of boron neutron capture therapy. Chin. Sci. Bull. **67**, 1490–1497 (2022). https://doi.org/10.1360/TB-2021-0844
7. A.Z. Diaz, Assessment of the results from the phase I/II boron neutron capture therapy trials at the Brookhaven National Laboratory from a clinician's point of view. J. Neuro Oncol. **62**, 101–109 (2003). https://doi.org/10.1017/BF02699937
8. R.L. Moss, Status of the BNCT project at the HFR Petten. Cancer Neutr. Capture Ther. (1996). https://doi.org/10.1007/978-1-4757-9567-7_40
9. S. Savolainen, M. Kortesniemi, M. Timonen et al., Boron neutron capture therapy (BNCT) in Finland: Technological and physical prospects after 20 years of experiences. Phys. Med. **29**, 233–248 (2013). https://doi.org/10.1016/j.ejmp.2012.04.008
10. J. Burian, S. Flibor, M. Marek et al., Physics for BNCT. J. Phys. Conf. Ser. **41**, 174–186 (2006). https://doi.org/10.1088/1742-6596/41/1/017
11. Y. Sakurai, H. Tanaka, T. Takata et al., Advances in boron neutron capture therapy (BNCT) at Kyoto university—From reactor-based BNCT to accelerator-based BNCT. J. Korean Phys. Soc. **67**, 76–81 (2015). https://doi.org/10.3938/jkps.67.76
12. L. Provenzano, R.O. Farías, J.M. Longhino et al., A prospective study to assess the performance of the improved boron neutron capture therapy facility in argentina. Appl. Radiat. Isot. **88**, 171–176 (2014). https://doi.org/10.1016/j.apradiso.2013.11.041
13. Y.H. Liu, P.E. Tsai, H.M. Liu et al., The angular and spatial distributions of the thermal neutron source description of the THOR BNCT beam. Radiat. Meas. **45**, 1432–1435 (2010). https://doi.org/10.1016/j.radmeas.2010.08.023
14. T. Kato, K. Hirose, H. Tanaka et al., Design and construction of an accelerator-based boron neutron capture therapy (AB-BNCT) facility with multiple treatment rooms at the Southern Tohoku BNCT Research Center. Appl. Radiat. Isot. **156**, 108961 (2020). https://doi.org/10.1016/j.apradiso.2019.108961
15. N. Hu, H. Tanaka, R. Kakino et al., Evaluation of a treatment planning system developed for clinical boron neutron capture therapy and validation against an independent Monte Carlo dose calculation system. Radiat. Oncol. **16**, 243 (2021). https://doi.org/10.1186/s13014-021-01968-2
16. H. Kumada, K. Takada, F. Naito et al., Beam performance of the iBNCT as a compact linac-based BNCT neutron source developed by University of tsukuba. AIP Conf. Proc. **2160**, 050013 (2019). https://doi.org/10.1063/1.5127705
17. L. Porra, T. Seppälä, L. Wendland et al., Accelerator-based boron neutron capture therapy facility at the Helsinki University Hospital. Acta Oncol. **61**, 269–273 (2022). https://doi.org/10.1080/0284186X.2021.1979646
18. J.Y. Chen, Z.L. Hu, J.F. Tong et al., Study of BNCT neutronics optimization for out-of-beam dosimetry based on radiobiological figures of merit. Nucl. Instrum. Meth. B **508**, 1–9 (2021). https://doi.org/10.1016/j.nimb.2021.09.014
19. J.Y. Chen, J.F. Tong, Z.L. Hu et al., Evaluation of neutron beam characteristics for D-BNCT01 facility. Nucl. Sci. Tech. **33**, 12 (2022). https://doi.org/10.1007/s41365-022-00996-1
20. Z.Z. Zhang, Y.Z. Chong, Y.H. Liu et al., A review of planned, ongoing clinical studies and recent development of BNCT in mainland of China. Cancers **15**, 4060 (2023). https://doi.org/10.3390/cancers15164060

21. L.X. Zhang, S.Z. Chen, Z.D. Zhang et al., Resolution analysis of thermal neutron radiography based on accelerator-driven compact neutron source. Nucl. Sci. Tech. **34**, 76 (2023). https://doi.org/10.1007/s41365-023-01227-x
22. L. Zhang, H.W. Yu, Y. Li et al., Improved formation density measurement using controllable D-D neutron source and its lithological correction for porosity prediction. Nucl. Sci. Tech. **33**, 26–36 (2022). https://doi.org/10.1007/s41365-022-00988-1
23. H.H. Xiong, Q.S. Zeng, Y.C. Han et al., Neutronics analysis of a subcritical blanket system driven by a gas dynamic trap-based fusion neutron source for ^{99}Mo production. Nucl. Sci. Tech. **34**, 49 (2023). https://doi.org/10.1007/s41365-023-01206-2
24. N. Colonna, L. Phair, L. Beaulieu et al., Exploring alternative (p, n) and (d, n) reactions for BNCT. AIP Conf. Proc. **475**, 1045 (1999). https://doi.org/10.1063/1.59099
25. S.N. Fu, T.J. Liang, H.S. Chen et al., Status and outlook: Research and development on the neutron source for BNCT. Chin. Sci. Bull. **67**, 1471–1478 (2022). https://doi.org/10.1360/TB-2021-1254
26. M. Wang, Y.P. Tong, The progress and prospect of Boron Neutron Capture Therapy. J. Isotop. **33**, 14–26 (2020). https://doi.org/10.7538/tws.2017.youxian.061
27. K. Yoshiaki, Accelerator-based neutron source for boron neutron capture therapy. Ther. Radiol. Oncol. **2**, 55 (2018). https://doi.org/10.21037/tro.2018.10.05
28. Los Alamos National Laboratory, MCNPX User's Manual Version 2.7.0 (2011)
29. Evaluated Nuclear Data File. ENDF/B-VIII.0 (2018). https://www.nndc.bnl.gov/endf/
30. C.K. Li, Y.J. Ma, X.B. Tang et al., Research of accelerator-based neutron source for boron neutron capture therapy. Nucl. Tech. (in Chinese) **36**, 090203 (2013). https://doi.org/10.11889/j.0253-3219.2013.hjs.36.090203
31. Z.Q. Guo, C.Q. Liu, W.Z. Zhang et al., Optimization design of BNCT neutron source and moderating body based on accelerator ^{7}Li(p, n) reaction. Nucl. Tech. (in Chinese) **45**, 050201 (2022). https://doi.org/10.11889/j.0253-3219.2022.hjs.45.050201
32. S.X. Gu, F.J. Cui, N.Y. Wang et al., Simulation of neutron moderating materials performance based on BNCT of 2.5 MeV proton accelerator. Nucl. Phys. Rev. **39**, 2021073 (2022). https://doi.org/10.11804/NuclPhysRev.39.2021073
33. Y.S. Tian, Design and optimizaiton of beam shaping assembly for accelerator-based boron neutron capture therapy. MA thesis (2018). https://kns.cnki.net/KCMS/detail/detail.aspx?dbname=CMFD201901&filename=1018264723.nh
34. Z.P. Wu, X.B. Jiang, W.S. Zhang et al., Monte Carlo simulation of neutron sensitivity of microfission chamber in neutron flux measurement. Nucl. Sci. Tech. **33**, 78 (2022). https://doi.org/10.1007/s41365-022-01062-6
35. IAEA, Current status of neutron capture therapy, IAEA-TEC-DOC-1223. International Atomic Energy Agency. (2001)
36. Y. Gong, X.C. Guan, Q. Wang et al., Design of moderator for boron neutron capture therapy based on D-D neutron source. Nucl. Tech. (in Chinese) **43**, 090303 (2020). https://doi.org/10.11889/j.0253-3219.2020.hjs.43.090303
37. ICRU, Photon, Electron, Proton and Neutron Interaction Data for Body Tissues. ICRU REPORT **46** (1992)
38. F. Rahmani, M. Shahriari, Dose calculation and in-phantom measurement in BNCT using response matrix method. Appl. Radiat. Isot. **69**, 1874–1877 (2011). https://doi.org/10.1016/j.apradiso.2011.02.019
39. P. Torres-Sánchez, I. Porras, N. Ramos-Chernenko et al., Optimized beam shaping assembly for a 2.1-MeV proton-accelerator-based neutron source for boron neutron capture therapy. Sci. Rep. **11**, 7576 (2021). https://doi.org/10.1038/s41598-021-87305-9
40. L. Deng, C.B. Chen, T. Ye et al., The dosimetry calculation for Boron Neutron Capture Therapy. InTech (2001). www.intechopen.com
41. L. Zaidi, M. Belgaid, R. Khelifi, Monte Carlo based dosimetry for neutron capture therapy of brain tumors. EPJ Web Conf. **128**, 04003 (2016). https://doi.org/10.1051/epjconf/201612804003
42. S. Rosidah, Y. Sardjono, Y. Sumardi, Dose analyze of boron neutron capture therapy (BNCT) at skin cancer melanoma using mcnpx with neutron source from thermal column of kartini reactor. Indones. J. Phys. Nucl. Appl. **2**, 111 (2017). https://doi.org/10.24246/ijpna.v2i3.111-123